View metadata, citation and similar papers at core.ac.uk

brought to you by CORE

provided by Universiti Teknologi Malaysia Institutional Repository

International Journal of Heat and Mass Transfer 121 (2018) 187–195

Contents lists available at ScienceDirect

International Journal of Heat and Mass Transfer

journal homepage: www.elsevier.com/locate/ijhmt

Flow characteristics of gaseous flow through a microtube discharged into the atmosphere

Chungpyo Hong [a,*], Goku Tanaka [a], Yutaka Asako [b], Hiroshi Katanoda [a]

[a] Department of Mechanical Engineering, Kagoshima University, 1-21-40 Korimoto, Kagoshima 890-0065, Japan
[b] Department of Mechanical Precision Engineering, Malaysia-Japan International Institute of Technology, University Technology Malaysia, Jalan Sultan Yahya Petra, 54100 Kuala Lumpur, Malaysia

ARTICLE INFO

Article history:
Received 21 October 2016
Received in revised form 25 August 2017
Accepted 21 December 2017
Available online 5 January 2018

Keywords:
Friction factor
Turbulent
Compressible gaseous flow
Microtube
Choked flow

ABSTRACT

Flow characteristics for a wide range of Reynolds number up to turbulent gas flow regime, including flow choking were numerically investigated with a microtube discharged into the atmosphere. The numerical methodology is based on the Arbitrary-Lagrangian-Eulerian (ALE) method. The LB1 turbulence model was used in the turbulent flow case. Axis-symmetric compressible momentum and energy equations of an ideal gas are solved to obtain the flow characteristics. In order to calculate the underexpanded (choked) flow at the microtube outlet, the computational domain is extended to the downstream region of the hemisphere from the microtube outlet. The back pressure was given to the outside of the downstream region. The computations were performed for adiabatic microtubes whose diameter ranges from 10 to 500 μm and whose aspect ratio is 100 or 200. The stagnation pressure range is chosen in such a way that the flow becomes a fully underexpanded flow at the microtube outlet. The results in the wide range of Reynolds number and Mach number were obtained including the choked flow. With increasing the stagnation pressure, the flow at the microtube outlet is underexpanded and choked. Although the velocity is limited, the mass flow rate (Reynolds number) increases. In order to further validate the present numerical model, an experiment was also performed for nitrogen gas through a glass microtube with 397 μm in diameter and 120 mm in length. Three pressure tap holes were drilled on the glass microtube wall. The local pressures were measured to determine local values of Mach numbers and friction factors. Local friction factors were numerically and experimentally obtained and were compared with empirical correlations in the literature on Moody's chart. The numerical results are also in excellent agreement with the experimental ones.

© 2018 Elsevier Ltd. All rights reserved.

1. Introduction

Advanced development to the design technology of MEMS (micro electro mechanical system) have increased the need for an understanding of fluid flow and heat transfer of micro flow devices such as micro-heat exchangers, micro-reactors and many other micro-fluid systems. Therefore numerous experimental and numerical studies have been performed in an effort to better understand flow characteristics in microchannels.

In the case of gaseous flow in microchannels, it is well known that the rarefaction, the surface roughness, and the compressibility significantly affect the flow characteristics separately or simultaneously [1]. For the microchannels with 10 μm or more in hydraulic diameter, the effect of compressibility is more dominant on flow characteristics than that of surface roughness and rarefaction. The compressibility effect leads that the flow accelerates along the length and the pressure steeply falls near the outlet due to gas expansion. Therefore to obtain the local value of friction factor is important for an understanding of flow phenomenon of gaseous flow in microchannels. The compressibility effect on laminar gas flow in microchannels have been numerically investigated by many researchers, e.g. Prud'homme et al. [2], Berg et al. [3], Kavehpour et al. [4], Guo et al. [5], Sun and Faghri [6]. Recently, Asako et al. [7,8] and Hong et al. [9–11] conducted numerical investigations of gas flow in microchannels. They obtained $f \cdot Re$ correlations as functions of Mach number and Knudsen number. The $f \cdot Re$ correlation obtained for rectangular microchannels are in excellent agreement with the experimental values of $f \cdot Re$ obtained by Hong et al. [12] who measured the local pressure along the channel length, to determine the local values of Mach number and friction factor for the range of $58 \leq Re \leq 7965$ for nitrogen.

* Corresponding author.
E-mail addresses: hong@mech.kagoshima-u.ac.jp (C. Hong), k3944613@kadai.jp (G. Tanaka), y.asako@utm.my (Y. Asako), katanoda@mech.kagoshima-u.ac.jp (H. Katanoda).

https://doi.org/10.1016/j.ijheatmasstransfer.2017.12.104
0017-9310/© 2018 Elsevier Ltd. All rights reserved.

Nomenclature

a	speed of sound [m/s]
D	microtube diameter [m]
i	specific internal energy [J/kg]
k	turbulence energy [m^2/s^2]
L	micro-tube length [m]
Ma	Mach number [–]
n	pressure port number
p	static pressure [Pa]
p^*	modified pressure, $= \overline{p} + \frac{2}{3}\overline{\rho}k$ [Pa]
r, x	coordinates [m]
R	gas constant [J/(kg·K)]
Re	Reynolds number [–]
T	static temperature [K]
t_u	turbulent intensity [–]
u, v	velocity components [m/s]
y^+	dimensionless wall distance [–]
δ^*	displacement thickness based on mass flow [m]
ε	turbulence dissipation rate [m^2/s^3]
γ	specific heat ratio [–]
λ	thermal conductivity [W/(m·K)]
λ_{eff}	effective thermal conductivity, $= \lambda + \lambda_t$ [W/(m·K)]
λ_t	turbulent thermal conductivity [W/(m·K)]
μ	viscosity [Pa·s]
μ_{eff}	effective viscosity, $= \mu + \mu_t$ [Pa·s]
μ_k	diffusion coefficient for k equation, $= \mu + \mu_t/\sigma_k$ [Pa·s]
μ_t	turbulent viscosity [Pa·s]
μ_ε	diffusion coefficient for ε equation, $= \mu + \mu_t/\sigma_\varepsilon$ [Pa·s]
ρ	density [kg/m^3]
σ	turbulent Prandtl number [–]
τ	shear stress [Pa]
τ_w	shear stress on wall [Pa]
ϕ	dissipation function [$1/s^2$]

Subscript

ave	cross sectional average value
in	inlet
out	outlet of micro-tube
stg	stagnation value

Superscript

¯	Reynolds-averaged value
~	Favre-averaged value

In the case of turbulent gas flow in microchannels, Chen et al. [13] performed numerical procedures to solve compressible, turbulent boundary-layer equations by using the Baldwin-Lomax two-layer turbulence model. The numerically calculated $f{\cdot}Re^{1/4}$ values are higher than those predicted by the Fanno line flow. Recently, Murakami and Asako [14] investigated numerically to obtain the effect of compressibility on the local pipe friction factors of laminar and turbulent gas flow in microtubes. They reported that the ratio of the Fanning friction factor to Blasius formula for turbulent flow is equal to unity but the ratio of the Darcy friction factor to Blasius formula is still a function of the Mach number. However, the Fanning friction factor of the turbulent flow in a PEEK microtube measured by Kawashima and Asako [15] is 12–20% higher than the value predicted from Blasius formula.

Attention will now be focused on choked flow in microchannels; the choked flow has been extensively investigated over the years under the conditions that the inlet pressure is preserved at a specific (atmospheric) pressure and the back pressure is decompressed. Lijo et al. [16] numerically investigated the effect of choking on flow and heat transfer in a microchannel whose hydraulic diameter is 300 μm. They considered the flow to be choked when the mass flow rate does not change with the conditions of a specific inlet pressure and a further decrease in the back pressure. They reported that for a higher-pressure ratio the Mach number near the exit of the channel is well above 1.0 since thinning boundary layer near the exit. On the other hand, in the case of atmospheric back pressure and the further increase in inlet pressure, the gas velocity becomes limited and the mass flow rate (Reynolds number) is increased. In this situation the outlet pressure of the channel is higher than the back pressure and the flow becomes underexpanded. Kawashima et al. [17] investigated numerically the Mach number and pressure at outlet plane of a straight microtube for both laminar and turbulent flow cases. They found that the Mach number at the outlet plane of the choked flow depends on the tube diameter and ranges from 1.16 to 1.25. However, details of choked (underexpanded) flow in a micro-tube are still open problems because of measurement limitation. There also seems to be no parametric study to investigate flow characteristics of non-choking and choking turbulent gas flows through a microtube discharged into atmosphere with an experimental validation. This is the motivation of the present numerical study with microtubes whose diameters range from 10 to 500 μm and whose aspect ratios are 100 and 200. In order to further validate the present numerical model, an experiment was also conducted with a glass microtube with 397 μm in diameter and 120 mm in length.

2. Description of the problem

The schematic diagram of gaseous flow in a microtube for numerical calculation is shown in Fig. 1. The numerical calculations were performed under the assumption that the flow is steady and axisymmetric and laminar or turbulent. Compressible fluid in a reservoir at the stagnation pressure, p_{stg} and the stagnation temperature, T_{stg}, passes through an adiabatic microtube into the atmosphere at the pressure, p_b (10^5 Pa). The calculational domain is extended to the downstream region of hemisphere to calculate the underexpanded flow as shown in Fig. 1. The physical quantities are the time mean values and the physical properties such as the viscosity and thermal conductivity of the fluid are assumed to be constant. For a microtube, the following governing equations are used [17]:

$$\frac{\partial \overline{\rho}\widetilde{u}}{\partial x} + \frac{1}{r}\frac{\partial \overline{\rho} r \widetilde{v}}{\partial r} = 0 \tag{1}$$

$$\frac{\partial \overline{\rho}\widetilde{u}\widetilde{u}}{\partial x} + \frac{1}{r}\frac{\partial \overline{\rho} r \widetilde{v}\widetilde{u}}{\partial r} = -\frac{\partial p^*}{\partial x} + \frac{\partial \tau_{xx}}{\partial x} + \frac{1}{r}\frac{\partial r \tau_{rx}}{\partial r} \tag{2}$$

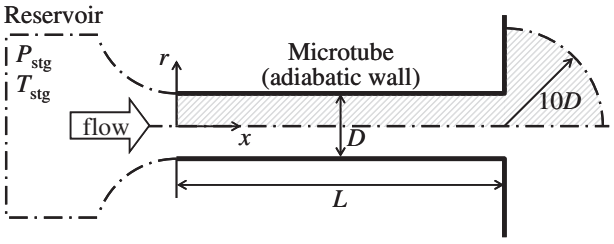

Fig. 1. Schematic diagram of a problem.

$$\frac{\partial \overline{\rho}\widetilde{u}\widetilde{v}}{\partial x}+\frac{1}{r}\frac{\partial \overline{\rho} r\widetilde{v}\widetilde{v}}{\partial r}=-\frac{\partial p^{*}}{\partial r}+\frac{\partial \tau_{xr}}{\partial x}+\frac{1}{r}\frac{\partial r\tau_{rr}}{\partial r}-\frac{\tau_{\theta\theta}}{r} \tag{3}$$

$$\frac{\partial \overline{\rho}\widetilde{u}\widetilde{i}}{\partial x}+\frac{1}{r}\frac{\partial \overline{\rho} r\widetilde{v}\widetilde{i}}{\partial r}=-p^{*}\left(\frac{\partial \widetilde{u}}{\partial x}+\frac{1}{r}\frac{\partial r\widetilde{v}}{\partial r}\right)+\mu_{\mathrm{eff}}\phi+\frac{\partial q_{x}}{\partial x}+\frac{1}{r}\frac{\partial rq_{r}}{\partial r} \tag{4}$$

where the viscous stresses are expressed as

$$\tau_{xx}=\mu_{\mathrm{eff}}\left\{2\frac{\partial \widetilde{u}}{\partial x}-\frac{2}{3}\left(\frac{\partial \widetilde{u}}{\partial x}+\frac{1}{r}\frac{\partial r\widetilde{v}}{\partial r}\right)\right\} \tag{5}$$

$$\tau_{rr}=\mu_{\mathrm{eff}}\left\{2\frac{\partial \widetilde{v}}{\partial r}-\frac{2}{3}\left(\frac{\partial \widetilde{u}}{\partial x}+\frac{1}{r}\frac{\partial r\widetilde{v}}{\partial r}\right)\right\} \tag{6}$$

$$\tau_{\theta\theta}=\mu_{\mathrm{eff}}\left\{2\frac{\widetilde{v}}{r}-\frac{2}{3}\left(\frac{\partial \widetilde{u}}{\partial x}+\frac{1}{r}\frac{\partial r\widetilde{v}}{\partial r}\right)\right\} \tag{7}$$

$$\tau_{xr}=\tau_{rx}=\mu_{\mathrm{eff}}\left(\frac{\partial \widetilde{v}}{\partial x}+\frac{\partial \widetilde{u}}{\partial r}\right) \tag{8}$$

and the heat fluxes caused by thermal conduction are

$$q_{x}=\lambda_{\mathrm{eff}}\frac{\partial \widetilde{T}}{\partial x},\quad q_{r}=\lambda_{\mathrm{eff}}\frac{\partial \widetilde{T}}{\partial r} \tag{9}$$

ϕ is the viscous dissipation function expressed as

$$\phi=2\left\{\left(\frac{\partial \widetilde{u}}{\partial x}\right)^{2}+\left(\frac{\widetilde{v}}{r}\right)^{2}+\left(\frac{\partial \widetilde{v}}{\partial r}\right)^{2}\right\}-\frac{2}{3}\left(\frac{\partial \widetilde{u}}{\partial x}+\frac{1}{r}\frac{\partial r\widetilde{v}}{\partial r}\right)^{2}+\left(\frac{\partial \widetilde{u}}{\partial r}+\frac{\partial \widetilde{v}}{\partial x}\right)^{2} \tag{10}$$

Also, the equation of state for the ideal gas can be expressed as

$$\widetilde{i}=\frac{1}{\gamma-1}\frac{\overline{p}}{\overline{\rho}}=\frac{R}{\gamma-1}\widetilde{T} \tag{11}$$

2.1. Turbulence model

The k-ε low Reynolds number model is used. In this model, the turbulence kinetic energy k and the turbulence dissipation rate ε are solved to determine the coefficient of turbulent viscosity μ_{t}. The various turbulence models have been proposed. In this paper, the Lam-Bremhorst low Reynolds number (LB1) model [18,19] is chosen since LB1 model is widely used and very stable.

$$\frac{\partial \overline{\rho}k\widetilde{u}}{\partial x}+\frac{1}{r}\frac{\partial \overline{\rho} rk\widetilde{v}}{\partial r}=P_{k}+\frac{\partial}{\partial x}\left(\mu_{k}\frac{\partial k}{\partial x}\right)+\frac{1}{r}\frac{\partial}{\partial r}\left(r\mu_{k}\frac{\partial k}{\partial r}\right)-\overline{\rho}\varepsilon \tag{12}$$

$$\frac{\partial \overline{\rho}\varepsilon\widetilde{u}}{\partial x}+\frac{1}{r}\frac{\partial \overline{\rho} r\varepsilon\widetilde{v}}{\partial r}=C_{\varepsilon 1}f_{1}\frac{\varepsilon}{k}P_{k}+\frac{\partial}{\partial x}\left(\mu_{\varepsilon}\frac{\partial \varepsilon}{\partial x}\right)+\frac{1}{r}\frac{\partial}{\partial r}\left(r\mu_{\varepsilon}\frac{\partial \varepsilon}{\partial r}\right)-C_{\varepsilon 2}f_{2}\overline{\rho}\frac{\varepsilon^{2}}{k} \tag{13}$$

$$P_{k}=\mu_{t}\phi-\frac{2}{3}\overline{\rho}k\left(\frac{\partial \widetilde{u}}{\partial z}+\frac{1}{r}\frac{\partial r\widetilde{v}}{\partial r}\right) \tag{14}$$

$$\mu_{t}=C_{\mu}f_{\mu}\overline{\rho}\frac{k^{2}}{\varepsilon},\quad \lambda_{t}=\frac{c_{p}\mu_{t}}{\sigma_{T}} \tag{15}$$

Constants and functions are

$$C_{\mu}=0.09,\quad \sigma_{k}=1.0,\quad \sigma_{\varepsilon}=1.3,\quad \sigma_{T}=0.9,$$
$$C_{\varepsilon 1}=1.44,\quad C_{\varepsilon 2}=1.92,$$

$$f_{1}=1+\left(\frac{0.05}{f_{\mu}}\right)^{3},\quad f_{2}=1-e^{-R_{T}^{2}},\quad f_{\mu}=\left(1-e^{-0.0165R_{y}}\right)^{2}\left(1-\frac{20.5}{R_{T}}\right),$$

$$R_{T}=\frac{\overline{\rho}k^{2}}{\varepsilon\mu},\quad R_{y}=\frac{\overline{\rho}\sqrt{k}y_{w}}{\mu} \tag{16}$$

These values are standard values of the model and y_{w} represents the minimum distance from the tube wall.

2.2. Boundary conditions

The effect of rarefaction is negligible because the tube diameter is much larger than the molecular mean free path. Therefore no-slip condition at the wall is used for velocity. The thermal boundary condition on the wall is adiabatic (not like isentropic flow, flow on an adiabatic tube wall will be called adiabatic flow hereinafter). It is also assumed that the velocity, pressure, temperature and density profiles at the inlet are uniform. From these assumptions, the boundary conditions are expressed as

$$\begin{aligned}
&\text{on the tube wall}: \quad u=v=k=0,\ \partial T/\partial r=\partial\varepsilon/\partial r=0\\
&\text{on the wall at the outlet plane}:\\
&\quad u=v=k=0,\ \partial T/\partial r=\partial\varepsilon/\partial r=0\\
&\text{on the symmetric axis}:\\
&\quad v=0,\ \partial u/\partial r=0,\ \partial T/\partial r=\partial k/\partial r=\partial\varepsilon/\partial r=0\\
&\text{at the inlet}: \quad v=0,\ u=u_{\mathrm{in}},\ p=p_{\mathrm{in}},\ \rho=\rho_{\mathrm{in}},\ T=T_{\mathrm{in}},\\
&\qquad\qquad k=k_{in},\ \varepsilon=\varepsilon_{in}\\
&\text{at the hemispheric outlet}: \quad p=p_{\mathrm{b}}
\end{aligned} \tag{17}$$

The values of velocity, pressure, temperature and density at the inlet are evaluated by the stagnation treatment proposed by Karki [20].

$$\frac{p_{\mathrm{in}}}{p_{\mathrm{stg}}}=\left(\frac{\rho_{\mathrm{in}}}{\rho_{\mathrm{stg}}}\right)^{\gamma}=\left(\frac{T_{\mathrm{in}}}{T_{\mathrm{stg}}}\right)^{\gamma/(\gamma-1)},\quad u_{\mathrm{in}}=\sqrt{\frac{2\gamma RT_{\mathrm{stg}}}{\gamma-1}\left\{1-\left(\frac{p_{\mathrm{in}}}{p_{\mathrm{stg}}}\right)^{(\gamma-1)/\gamma}\right\}} \tag{18}$$

k and ε at the inlet is determined in terms of the turbulent intensity, t_{u}, as

$$k_{\mathrm{in}}=1.5(t_{u}u_{\mathrm{in}})^{2},\quad \varepsilon_{\mathrm{in}}=0.1\ k_{\mathrm{in}}^{2} \tag{19}$$

and $t_{u}=0.014$ was used for all computations.

The working fluid was assumed to be a nitrogen gas. The thermophysical properties of $R=296.7$ J/(kg·K), $\gamma=1.399$, $\lambda=0.026$ W/(m·K) and $\mu=1.787$ Pa·s were used for computations.

2.3. Dimensionless valuables

Attention will now be focused on the calculation of the Reynolds number and Mach number that will be defined as

$$Re=\frac{u_{\mathrm{ave}}D}{\mu/\rho_{\mathrm{ave}}},\quad Ma_{\mathrm{ave}}=\frac{u_{\mathrm{ave}}}{a_{\mathrm{ave}}} \tag{20}$$

where D is a tube diameter and u_{ave}, ρ_{ave}, a_{ave} and i_{ave} are the cross sectional average velocity, density, speed of sound and specific internal energy as

$$u_{\mathrm{ave}}=\frac{8}{d^{2}}\int_{0}^{d/2}r\widetilde{u}dr,\quad \rho_{\mathrm{ave}}=\int_{0}^{d/2}\overline{\rho}r\widetilde{u}dr\Big/\int_{0}^{d/2}r\ \widetilde{u}\ dr$$

$$p_{\mathrm{ave}}=\frac{8}{d^{2}}\int_{0}^{d/2}r\overline{p}dr,\quad a_{\mathrm{ave}}=\sqrt{\gamma(\gamma-1)i_{\mathrm{ave}}},\quad i_{\mathrm{ave}}=\frac{1}{\gamma-1}\frac{p_{\mathrm{ave}}}{\rho_{\mathrm{ave}}},\quad T_{\mathrm{ave}}=\frac{p_{\mathrm{ave}}}{R\,\rho_{\mathrm{ave}}} \tag{21}$$

Note that the Re is constant along the tube but the Ma_{ave} varies in the flow direction.

The product of friction factor and Reynolds number is called Poiseuille number for laminar flow regime. The friction factors based on the Darcy's and Fanning definitions will be introduced. The Darcy friction factor is defined as

$$f_d = \frac{-2D}{\rho_{ave} u_{ave}^2}\left(\frac{dp_{ave}}{dx}\right) \tag{22}$$

The modified Fanning friction factors (four times of Fanning friction factor) is based on the wall shear stress and is defined as

$$f_f = \frac{4\tau_w}{(1/2)\rho_{ave} u_{ave}^2} = \frac{4\mu(\partial u/\partial r)_{r=0.5D}}{(1/2)\rho_{ave} u_{ave}^2} \tag{23}$$

2.4. Numerical simulation

The simulation code used is SALE [21]. The methodology of the code is based on the ALE (Arbitary-Langrangian-Eulerian) method. The detailed description of the ALE method is documented in the literature by Amsden et al. [21] and will not be presented here. In SALE, the computational domain is divided into quadrilateral cells. The velocity components are assigned at the vertices of the cell and the other values such as pressure, specific internal energy (temperature), and density are assigned at the cell centers. The cell size for all diameter gradually increased as the power of the spacing number [22] in the x-direction to $x/L = 0.8$, and it gradually decreased to the outlet of the tube. The number of the cells in x-direction in the tube section is 200 and the index of the power-law spacing is 1.8 in all case. The cell size gradually increased again in the radial direction of the hemispheric downstream section. The number of the cell in the downstream section in the radial direction is 300 for all diameters. The Low-Reynolds number turbulence mode requires sufficiently small cell near the tube wall. The cell size in r-direction gradually increased as the power of the spacing number form the tube wall to the center of the tube. The cell centers adjacent to the tube wall are placed in such a way that the dimensionless wall distance of the grid point y^+, defined as

$$y^+ = \frac{y_w \overline{\rho}}{\mu}\sqrt{\frac{\tau_w}{\overline{\rho}}} \tag{24}$$

is less than 2 and least two cell centers are allocated in the viscous sub layer. The number of the grids in r-direction is 40 for all diameters. The index of the power-law spacing is 1.2 for $D \leq 100$ μm and for 1.4 for $D \geq 250$ μm, respectively. The effects of cell size, downstream size and thermal boundary condition of tube wall on flow characteristics are well documented in Ref. [17].

3. Results and discussion

Numerical computations were conducted for microtubes of D = 10, 20, 50, 100, 250 and 500 μm whose aspect ratio is 100 and 200. All the computations were performed as laminar flow or turbulent flow. The tube diameter, the tube length, the stagnation pressure and the corresponding Reynolds number are listed in Table 1.

3.1. Mach number, temperature and pressure

The contour plots of Mach numbers and temperatures in the tube and its downstream region of D = 100 μm and L = 0.02 m are represented in Figs. 2 and 3, respectively. These are typical contour plots of Mach numbers and temperatures for fast flow ($Ma > 0.3$). As seen in Fig. 2 the flow is accelerated and the Mach number increases near the outlet due to gas expansion caused by the pressure drop. Therefore, the temperature decreases can be seen near the outlet due to thermal energy conversion into kinetic energy as shown in Fig. 3. Since the contour plots of Mach number and temperature for p_{stg} = 1200 and 1600 kPa are almost the same as shown in Figs. 2(b) and (c) and 3(b) and (c), the flow is choked and underexpanded at the outlet. Fig. 4 shows the pressure variations for all cases of D = 100 μm and L = 0.02 m. The pressure in the figure is the average value at a cross-section. The pressure curve becomes increasingly nonlinear as the stagnation pressure increases. The pressure falls steeply near the outlet due to the flow acceleration and gas expansion. The pressure at the outlet ($p_{stg} \geq$ 500 kPa) is higher than back pressure (100 kPa) since the flow at the outlet is choked (underexpanded). The Mach number is represented in Fig. 5. It is the average value at a cross-section. The Mach number increases along the tube length due to the flow acceleration. It also increases with increasing stagnation pressure. And it is very slightly increases at $p_{stg} \geq$ 500 kPa since the flow at the outlet becomes underexpanded and choked. The Mach number at the outlet for some cases exceeds the speed of sound.

The outlet Mach numbers obtained for all computations are plotted as a function of Reynolds number in Fig. 6. They are the average values at the outlet cross-section. The outlet Mach number increases with increasing Reynolds number and levels off at the Reynolds number where the flow is choked. Then, the outlet Mach numbers for all diameters are more than unity. The outlet Mach number of the smaller diameter reaches a higher maximum value at a smaller Reynolds number. The microtubes with the same diameter and different aspect ratio have almost the same outlet Mach number at an arbitrary Reynolds number. In the case of D = 10 and 20 μm, the flow is choked in the laminar flow regime. And the outlet Mach number leveled off, then decreases around Re = 2300 and levels off since the velocity profile at a cross section becomes flatter due to the flow transition from laminar to turbulent. As a result of that, the outlet Mach number with flow choking is more than unity and depends on the diameter. The Mach number on the outlet plane of a microtube was discussed in detail in our previous study [17].

If a tube flow of the fluid with very high thermal conductivity can be considered, the fluid flow becomes isothermal, which the fluid inside the tube has almost the same temperature.

Therefore, in order to compare the outlet Mach number obtained by adiabatic flow (the present study) with that obtained by isothermal flow, supplement runs were performed with isothermal flow condition of T = 300 K at tubes of D = 20, 100 and 500 μm. The obtained outlet Mach numbers for isothermal flow are also plotted in Fig. 6 by the black colored symbols. They increase with increasing Reynolds number and level off with similar trends of those of adiabatic flow. However, the values obtained by isother-

Table 1
Tube diameter, length, p_{stg} and Re.

D (μm)	L (m)	p_{stg} (kPa)	Re	D (μm)	L (m)	p_{stg} (kPa)	Re
10	0.001	500–4000	117–4848	100	0.01	200–1000	994–7073
	0.002	300–9000	22–4957		0.02	300–1800	669–10,657
20	0.002	500–3000	384–4073	250	0.025	200–1000	3095–19,079
	0.004	500–5500	234–6182		0.05	125–1200	809–18,403
50	0.005	200–900	330–2842	500	0.05	200–500	6676–19,081
	0.01	200–1800	193–4930		0.1	105–800	174–24,926

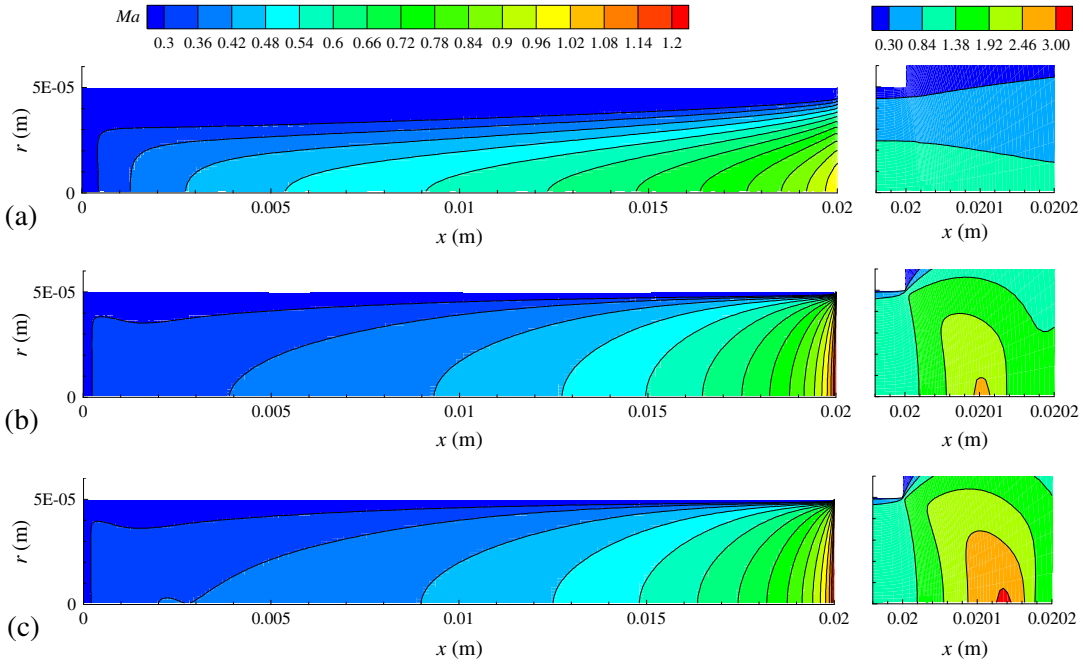

Fig. 2. Contour plots of Mach number for D = 100 μm and L = 0.02 m: (a) p_{stg} = 300 kPa (Re = 1414 and $Ma_{ave,\ out}$ = 0.587), (b) p_{stg} = 1200 kPa (Re = 6817 and $Ma_{ave,\ out}$ = 1.230), (c) p_{stg} = 1600 kPa (Re = 9322 and $Ma_{ave,\ out}$ = 1.238).

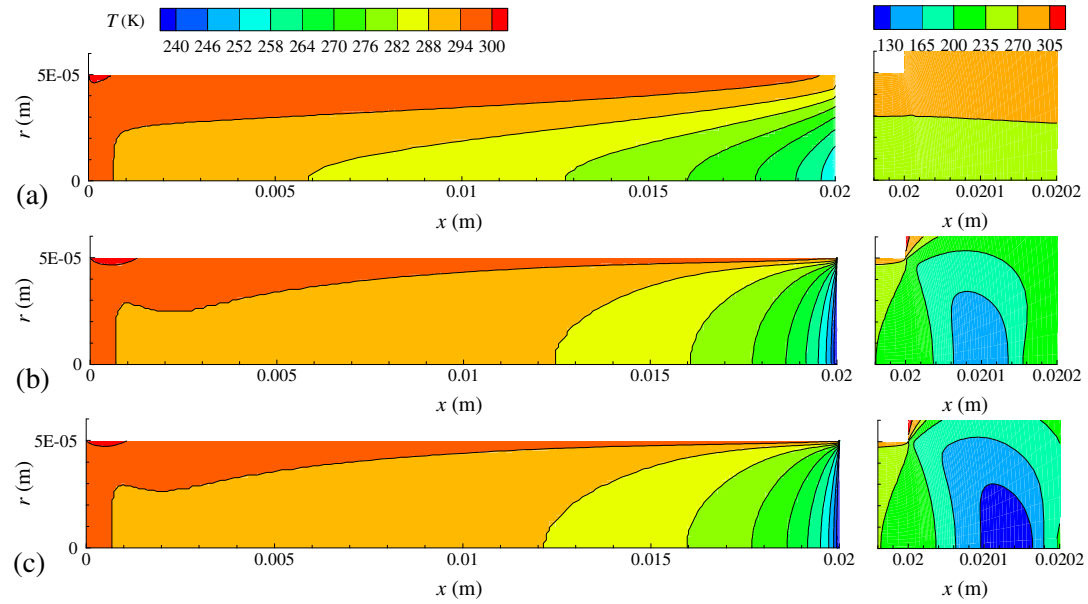

Fig. 3. Contour plots of temperature for D = 100 μm and L = 0.02 m: (a) p_{stg} = 300 kPa (Re = 1414 and $Ma_{ave,\ out}$ = 0.587), (b) p_{stg} = 1200 kPa (Re = 6817 and $Ma_{ave,\ out}$ = 1.230), (c) p_{stg} = 1600 kPa (Re = 9322 and $Ma_{ave,\ out}$ = 1.238).

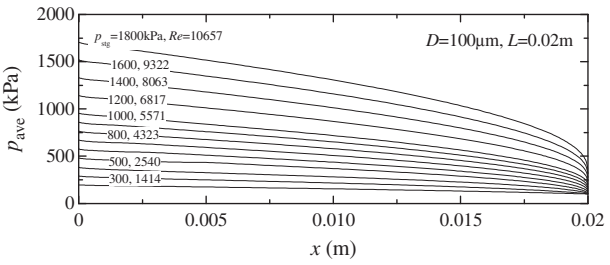

Fig. 4. Pressure as a function of x for D = 100 μm and L = 0.02 m.

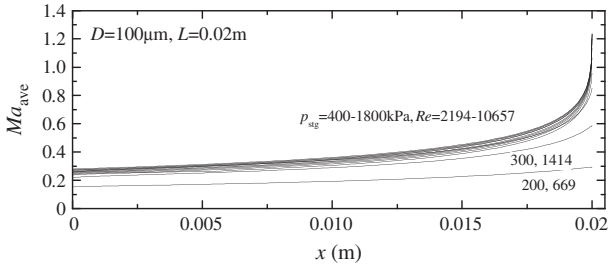

Fig. 5. Mach number as a function of x for D = 100 μm and L = 0.02 m.

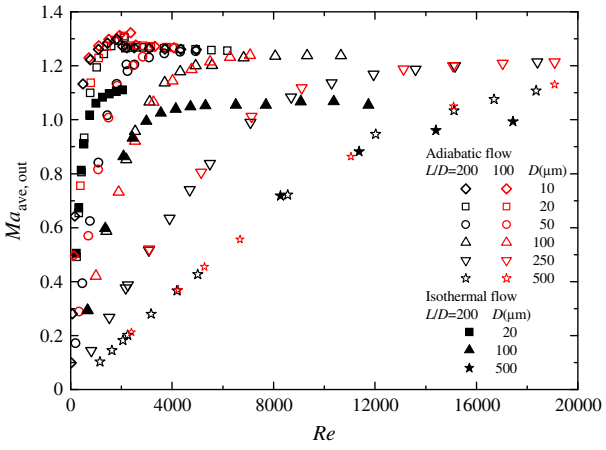

Fig. 6. Outlet Mach number as a function of *Re*.

mal flow are lower than those obtained by adiabatic flow (the present study) since the speed of sound does not include the effect of temperature decrease as seen in Fig. 3. However the values obtained by isothermal flow leveled off are slightly higher than unity. Fig. 7 represents curves of the average Mach number, velocity and speed of sound at a cross section for D = 100 μm and L = 0.02 m obtained under both the adiabatic and isotherm flows. The curve of the average velocity for isothermal flow coincides with that for the adiabatic flow. However, the values of speed of sound for isothermal flow are constant along the length and those for the adiabatic flow decrease near the outlet with decreasing temperature as seen in Fig. 3. As a result of that, Mach number of isothermal flow is lower than that of the adiabatic flow. If the thermal conductivity of the gas is extremely high, the flow is almost close to isothermal flow. However in actual situations, the flow seems to be closer to the adiabatic flow without heat input from the wall.

The average Mach number curves at a cross section obtained for microtubes with the same diameter and different length are plotted in Fig. 8 as a function of x/L. One case is for the laminar flow regime (Fig. 8(a)) and the other case is for turbulent one (Fig. 8 (b)). The Reynolds number for each case is almost the same, but the stagnation pressure of the longer microtube is lower than that of the shorter one. As seen in both figures Mach number curves rise in parallel until they reach $x/L \approx 0.9$, then they become the same since at the outlet Mach number is a function of mass flow rate (Reynolds number) and tube diameter due to the outlet faced to the atmosphere. As mentioned above, the outlet Mach number on the outlet plane of the choked flow is only a function of tube diameter [17].

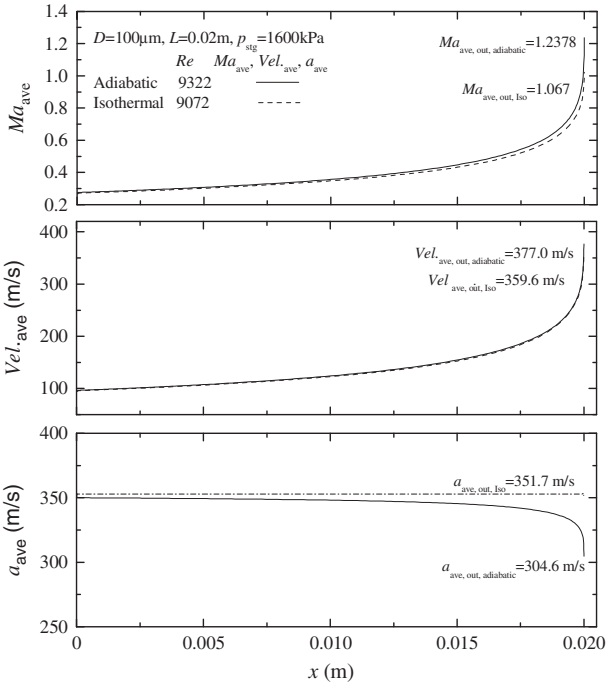

Fig. 7. Mach number, velocity and speed of sound as a function of *x*.

3.2. Friction factor

Fanning friction factor, f_f for all computations except D = 10 μm was obtained by Eq. (23). The values of the product of Fanning friction factor and Reynolds number, $f_f \cdot Re$ at $0.8L$ are plotted as a function of the Mach number at a cross sectional average in Fig. 9. In the case of laminar flow regime, the values increased with increasing Mach number since compressibility effect is dominant due to flow acceleration. Hong et al. [10] numerically obtained the $f_f \cdot Re$

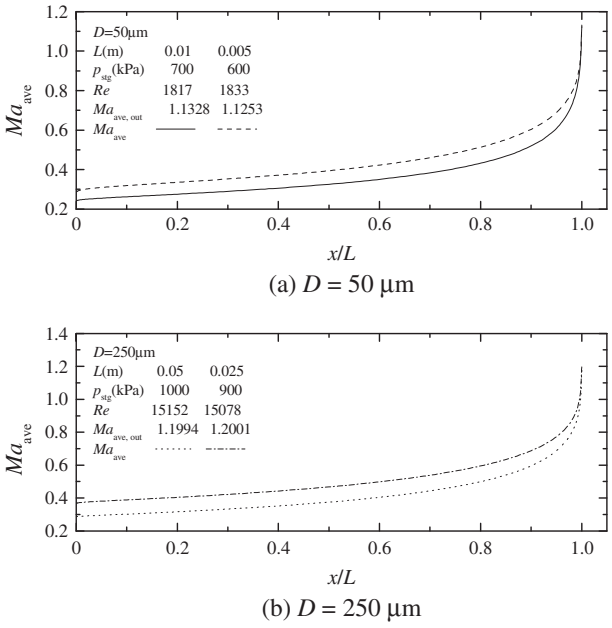

Fig. 8. Mach number as a function of *x*/*L*.

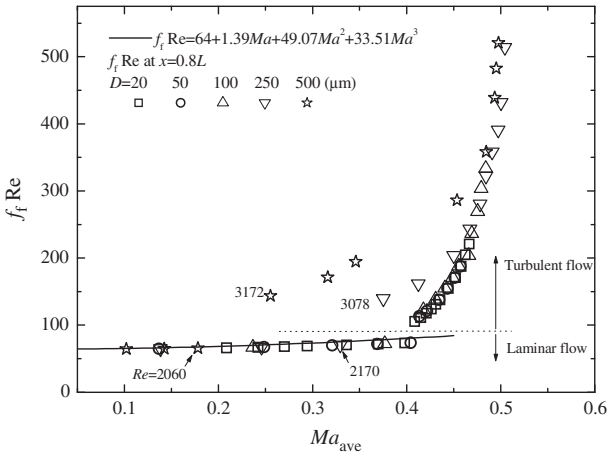

Fig. 9. $f_f \cdot Re$ as a function of *Re*.

correlation for a circular microtube as a quadratic function of Mach number. The solid line in the figure represents the $f_f \cdot Re$ correlation. The present results for all computation coincide with the $f_f \cdot Re$ correlation. In the case of turbulent regime, the values of $f_f \cdot Re$ increase with a large slope in deviation from the solid line. And they increase steeply because the flow is choked. This means that the gas velocity at each location remains nearly constant although the Reynolds number increase as shown in Fig. 6.

The values of Fanning and Darcy friction factor, f_f and f_d, at 0.4L, 0.6L, 0.8L and 0.9L obtained for D = 250 μm and L = 0.05 m are plotted on Moody's chart in Fig. 10. The corresponding Mach number at each location is also plotted in the figure. The solid line and dotted line in the figure represent the values obtained from $f = 64/Re$ and $f = 0.3164Re^{-0.25}$ (Blasius formula) for incompressible flow, respectively. As shown in the laminar flow regime, in the case of Ma < 0.2 (slow flow), both values of f_f and f_d are slightly higher than those of incompressible flow theory ($f = 64/Re$). The difference between f_f and f_d for the range from x = 0.4L to 0.9L is small because the Mach numbers in the range are almost the same. However in the case of Ma > 0.2, they deviate more and more from that of an incompressible flow and the difference between f_f and f_d is larger than that of Ma < 0.2 because the Mach number from x = 0.4L to 0.9L increase due to the compressibility effect.

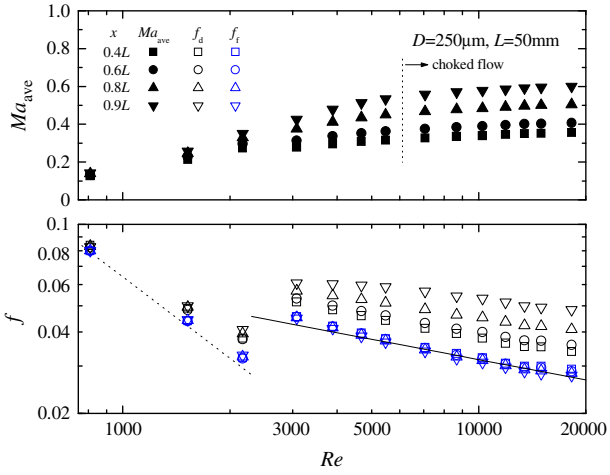

Fig. 10. Mach number and f on Moody chart.

As seen in the turbulent flow regime, the values of f_f closely coincide with the Blasius formula and might be only a function of Reynolds number. The compressibility (Mach number) effect including the choked flow on f_f is quite small. However the values of f_d deviate from those of Blasius formula with increasing Mach number. And they are parallel to those of Blasius formula in the range of Re > 6000 because of flow choking. Qualitatively similar results for the microtube of D = 10, 20, 50, 100 and 500 μm are obtained.

3.3. Validation with experimental data

In order to further validate the present numerical model, an experimental investigation whose setup was analogous to that of Kawashima et al. [15] was performed for nitrogen gas through a glass microtube with 397 μm in diameter and 12 cm in length. The picture of the cross section of the microtube is shown in Fig. 11(a). In order to measure the roughness of inner surface of the tube, a part of the microtube is cut and the picture of a cut tube is shown in Fig. 11(b). The microscopic image of its roughness feature (surface morphology) is also shown in Fig. 11(c), where the image is typical of all test sections used in the present study. The arithmetic mean height of the surface (S_a) of the glass microtube was measured with a 3D laser scanning confocal microscope for profilometry (Keyence VK-X260, Display resolution: 1 nm). The

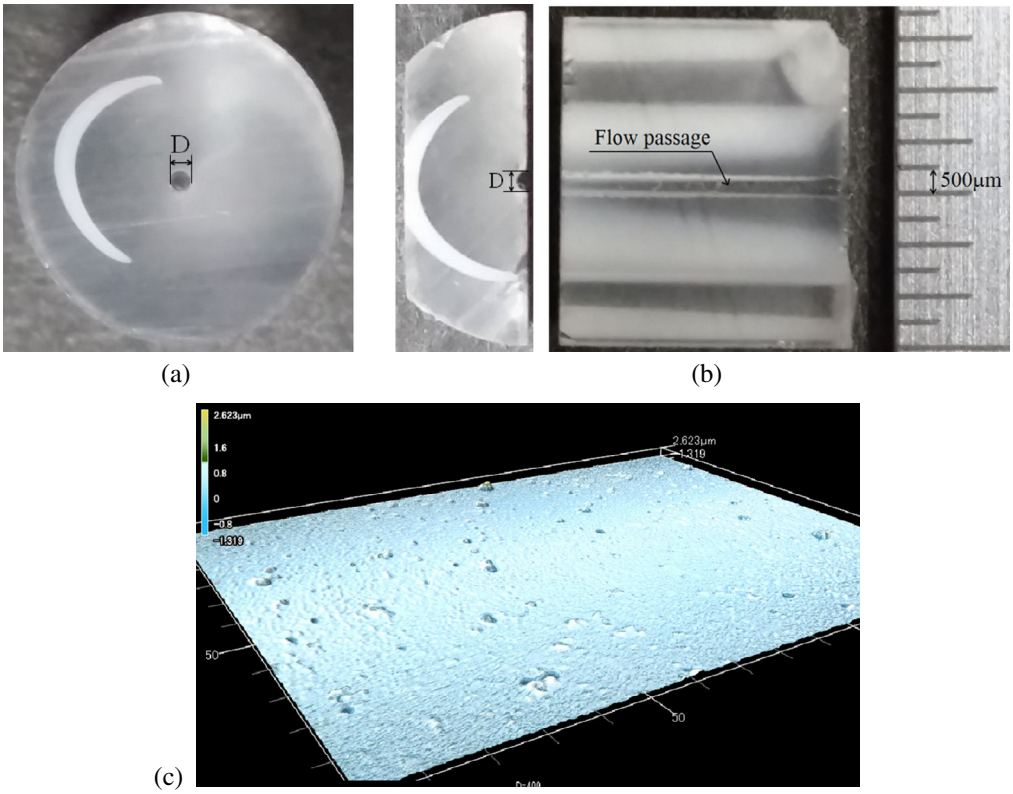

Fig. 11. Pictures of a glass microtube: (a) cross section, (b) cut tube, (c) microscopic image of its roughness feature.

arithmetic mean height of the tube (S_a) was around 0.073 μm, and relative roughness which is the ratio of the S_a and the diameter was about 0.0002%. Therefore the glass microtube is seemed to be smooth. Three pressure tap holes near the outlet were drilled as shown in Fig. 12. The local pressures were measured to determine the local values of Mach number and friction factor. Supplementary runs were also conducted for 6 cases whose tube dimensions coincide with those of the experiment. Since the thermal boundary condition of the computation is adiabatic, the glass microtube tested in the present study was covered with a foamed polystyrene to avoid heat gain and loss from the surroundings. The measured pressures at the pressure tap holes are plotted Fig. 13 as a function of x. The stagnation pressure is the curve parameter and the curves of the pressure are plotted for every 100 kPa. The pressures at the inlet that are obtained by solving Eq. (18) are also plotted in the figure. Numerically obtained pressures are also plotted in the figure by solid lines. Note that the pressure at the outlet of the tube (x = 0.12 m) is higher that the back pressure (p_b = 100 kPa) in the case of $p_{stg} \geq 400$ kPa. Both experimentally measured pressures and numerically obtained ones almost agree well. Experimentally and numerically obtained mass flow rates and Mach numbers at x = 0.09, 0.1 and 0.11 m and are plotted as a function of the stagnation pressure in Fig. 14. The numerical Mach numbers were obtained by Eq. (20) and the experimental ones were obtained with the local static gas temperature determined by the measured local pressure. The white symbols represent numerical results and the black symbols represent experimental ones. Mach number increases with increasing stagnation pressure and levels off in the range $p_{stg} \geq 400$ kPa. This is the reason why the flow is choked in that range. Both experimental and numerical mass flow rate and local Mach number are in excellent agreement.

The quasi-local Fanning friction factor between pressure tap holes for Fanno flow can be expressed with Eq. (23) as [15]

$$f_f = \frac{4\tau_w}{(1/2)\rho_{ave}u_{ave}^2} = \frac{2D}{x_{n+1}-x_n}\left[\frac{p_{ave,n}^2 - p_{ave,n+1}^2}{R(T_{ave,n}+T_{ave,n+1})} - \ln\left(\frac{p_{ave,n}}{p_{ave,n+1}}\right) - \ln\left(\frac{T_{ave,n}}{T_{ave,n+1}}\right)\right] \quad (25)$$

Both experimental and numerical values of the quasi-local Fanning friction factors were obtained from Eq. (25) between x = 9 cm

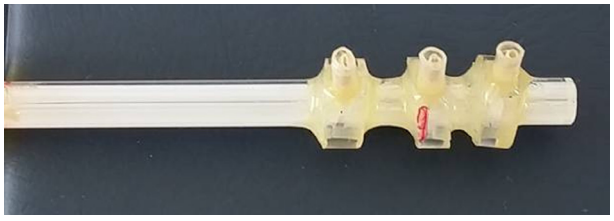

Fig. 12. Picture of pressure tap holder.

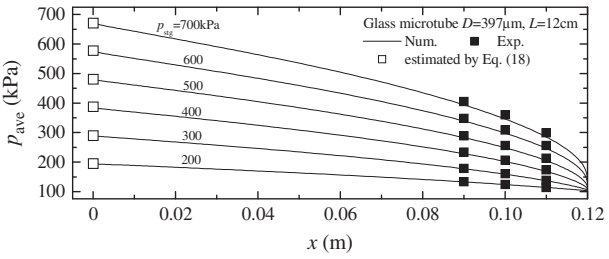

Fig. 13. Pressure distributions as a function of x.

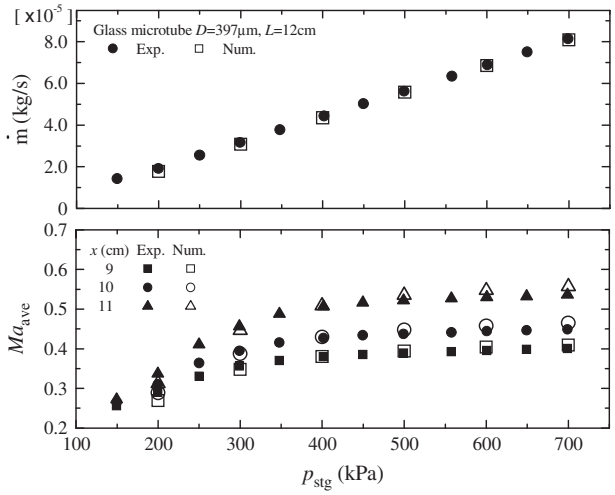

Fig. 14. Mass flow rates and Mach numbers as a function of stagnation pressure.

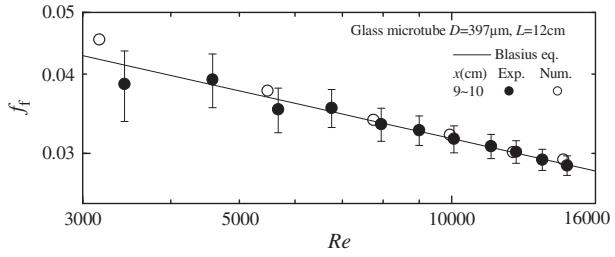

Fig. 15. f_f on Moody chart.

and 10 cm. They are also plotted in Fig. 15 as a function of Reynolds number on Moody chart. The solid line represents Blasius formula. Both of them nearly coincide with Blasius formula. As mentioned above, the Fanning friction factor in the turbulent flow regime coincides with Blasius formula and it is not a function of Mach number since the compressibility effect including the choked flow on the Fanning friction factor is quite small. It is noteworthy that both experimentally and numerically obtained quasi local Fanning friction factors of a flow in microtubes with a smooth inner surface discharged into the atmosphere are in good agreement with Blasius formula in the turbulent flow regime including the choked flow, showing the validity to the present numerical model.

4. Conclusion

Numerical investigations to obtain flow characteristics for a wide range of Reynolds number ($22 \leq Re \leq 24{,}926$) up to the turbulent gas flow regime including the choked flow were performed for microtubes whose inner diameters are 10, 20, 50, 100, 200 and 500 μm and whose aspect ratio is 100 or 200 in the case of atmospheric back pressure and the case of further increases in inlet pressure with an experimental validation. The following conclusions were reached.

(1) The Fanning friction factor, flow rate and pressure drop of the turbulent flow in a microtube with a smooth surface can be estimated from Blasius formula. Measured quasi-local Fanning friction factors are in good agreement with Blasius formula in the range of $3167 \leq Re \leq 14{,}581$ including the choked flow. The values of mass flow rates, local pressures, local Mach numbers and quasi-local Fanning friction factors obtained experimentally for a glass microtube of D

= 397 μm and L = 120 mm with a smooth inner surface nearly coincide with those obtained numerically under same conditions.

(2) The correlation between f_f·Re and Mach number can be physically explained. This is, the values of f_f·Re in the turbulent flow regime increase with a large slope in deviation from the f_f·Re correlation obtained for the laminar flow regime as Mach number increases. And they increase steeply due to flow choking where the Mach number stays constant but Reynolds number increases.

(3) In the case of the unchoked flow, the outlet Mach numbers of the flow in microtubes with the same diameter and different lengths are identical when Reynolds numbers of the flow are identical. And in the case of the choked flow, they have identical outlet Mach numbers depending on the microtube diameters.

Conflict of Interest

Authors declare that there is no conflict of interest.

References

[1] C. Hong, Y. Asako, J.-H. Lee, Poiseuille number correlation for high speed microflows, J. Phys. D Appl. Phys. 41 (2008), p. 105111(1-10).
[2] R.K. Prud'homme, T.W. Chapman, J.R. Bowen, Laminar compressible flow in a tube, Appl. Sci. Res. 43 (1986) 67–74.
[3] H.R. Berg, C.A. Seldam, P.S. Gulik, Compressible laminar flow in a capillary, J. Fluid Mech. 246 (1993) 1–20.
[4] H.P. Kavehpour, M. Faghri, Y. Asako, Effects of compressibility and rarefaction on gaseous flows in microchannels, Numer. Heat Transfer, Part A 32 (1997) 677–696.
[5] Z.Y. Guo, X.B. Wu, Compressibility effect on the gas flow and heat transfer in a micro tube, Int. J. Heat Mass Transfer 40 (13) (1997) 3251–3254.
[6] H. Sun, M. Faghri, Effect of rarefaction and compressibility of gaseous flow in micro channel using DSMC, Numer. Heat Transfer, Part A 38 (1999) 153–158.
[7] Y. Asako, K. Nakayama, T. Shinozuka, Effect of compressibility on gaseous flows in a micro-tube, Int. J. Heat Mass Transfer 48 (2005) 4985–4994.
[8] Y. Asako, T. Pi, S.E. Turner, M. Faghri, Effect of compressibility on gaseous flows in micro-channels, Int. J. Heat Mass Transfer 46 (2003) 3041–3050.
[9] C. Hong, Y. Asako, S.E. Turner, M. Faghri, Friction factor correlations for gas flow in slip flow regime, J. Fluids Eng. 129 (2007) 1268–1276.
[10] C. Hong, Y. Asako, M. Faghri, J.-H. Lee, Poiseuille number correlations for gas slip flow in micro-tubes, Numer. Heat Transfer, Part A 56 (2009) 785–806.
[11] C. Hong, Y. Asako, K. Suzuki, M. Faghri, Frction factor correlations for compressible gaseous flow in a concentric micro annular tube, Numer. Heat Transfer, Part A 61 (2012) 163–179.
[12] C. Hong, T. Yamada, Y. Asako, M. Faghri, Experimental investigation of laminar, transitional and turbulent gas flow in microchannels, Int. J. Heat Mass Transfer 55 (2012) 4397–4403.
[13] C.S. Chen, W.J. Kuo, Numerical study of compressible turbulent flow in microtubes, Numer. Heat Transfer, Part A 45 (2004) 85–99.
[14] S. Murakami, Y. Asako, Local pipe friction factor of compressible laminar or turbulent flow in micro-tubes, 9th International Conference on Nanochannels, Microchannels, and Minichannels, ICNMM2011-58036, 2011.
[15] D. Kawashiam, Y. Asako, Measurement of quasi-local friction factor of gas flow in a micro-tube, J. Mech. Eng. Sci. 230 (5) (2016) 782–792.
[16] V. Lijo, H.D. Kim, T. Setoguchi, Effects of choking on flow and heat transfer in micro-channels, Int. J. Heat Mass Transfer 55 (4) (2012) 701–709.
[17] D. Kawashima, T. Yamada, C. Hong, Y. Asako, Mach number at outlet plane of a straight micro-tube, J. Mech. Eng. Sci. 230 (19) (2016) 3420–3430.
[18] C.K.G. Lam, K. Bremhorst, A modified form of the k-ε model for predicting wall turbulence, ASME J. Fluid Eng 103 (1981) 456–460.
[19] V.C. Patel, W. Rodi, G. Scheuerer, Turbulence models for near-wall and low Reynolds number flows: a review, AIAA J. 23–9 (1984) 1308–1319.
[20] K.C. Karki, A Calculation Procedure for Viscous Flows at All Speeds in Complex Geometries PhD Thesis, University of Minnesota, 1986.
[21] A.A. Amsden, H.M. Rupell, C.W. Hire, SALE a Simplified ALE Computer Program of Fluid Flow at All Speeds, Los Alamos Scientific Lab Rep., LA-8095, 1980.
[22] S.V. Patankar, Computation of Conduction and Duct Flow Heat Transfer, Innovative Research, Inc., Minnesota, 1991.